AIMS Mathematics, 9(2): 4707–4728.
DOI: 10.3934/math.2024227
Received: 19 September 2023
Revised: 03 January 2024
Accepted: 08 January 2024
Published: 19 January 2024

http://www.aimspress.com/journal/Math

Research article

Artificial intelligence (AI) based neural networks for a magnetized surface subject to tangent hyperbolic fluid flow with multiple slip boundary conditions

Khalil Ur Rehman[1,*], Wasfi Shatanawi[1,2,*] and Zead Mustafa[2]

[1] Department of Mathematics and Sciences, College of Humanities and Sciences, Prince Sultan University, Riyadh, 11586, Saudi Arabia
[2] Department of Mathematics, Faculty of Science, The Hashemite University, P.O. Box 330127, Zarqa, 13133, Jordan

* **Correspondence:** Email: kurrehman@psu.edu.sa, wshatanawi@psu.edu.sa.

Abstract: In this paper, the Levenberg-Marquardt backpropagation scheme is used to develop a neural network model for the examination of the fluid flow on a magnetized flat surface with slip boundaries. The tangent hyperbolic fluid is considered along with heat generation, velocity, and thermal slip effects at the surface. The problem is modelled in terms of a non-linear differential system and Lie symmetry is used to get the scaling group of transformation. The order reduction of differential equations is done by using Lie transformation. The reduced system is solved by the shooting method. The surface quantity, namely skin friction, is evaluated at the surface for the absence and presence of an externally applied magnetic field. A total of 88 sample values are estimated for developing an artificial neural network model to predict skin friction coefficient (SFC). Weissenberg number, magnetic field parameter, and power law index are considered three inputs in the first layer, while 10 neurons are taken in the hidden layer. 62 (70%), 13 (15%), and 13 (15%) samples are used for training, validation, and testing, respectively. The Levenberg-Marquardt backpropagation is used to train the network by entertaining the random 62 sample values. Both mean square error and regression analysis are used to check the performance of the developed neural networking model. The SFC is noticed to be high at a magnetized surface for power law index and Weissenberg number.

Keywords: artificial intelligence; neural networks; tangent hyperbolic fluid; Lie symmetry; heat generation
Mathematics Subject Classification: 35A25, 65MO6, 76D05

Nomenclature

(X,Y)	Space variables	(U,V)	Velocity components
Γ	Time dependent material constant	m	Power law index
B	Magnetic field strength	ρ	Fluid density
Q_1	Heat generation coefficient	c_p	Specific heat at constant pressure
T	Fluid temperature	T_∞	Ambient temperature
σ	Fluid electrical conductivity	k	Thermal conductivity
ν_1	Kinematic viscosity	C	Fluid concentration
L_1	Velocity slip factor	D_1	Thermal slip factor
D_c	Mass diffusivity	b	Stretching rate
C_w	Surface concentration	θ_{tem}	Dimensionless temperature
C_∞	Ambient concentration	T_w	Surface temperature
ε	Small parameter	$A_{k=1...6}$	Real numbers
ϕ_{con}	Dimensionless concentration	Ψ	Stream function
β_1	Velocity slip parameter	β_2	Thermal slip parameter
$F'(\chi)$	Dimensionless fluid velocity	W_n	Weissenberg number
Pr	Prandtl number	H_a	Magnetic field parameter
H^+	Heat generation parameter	Sc	Schmidt number

1. Introduction

The study of non-Newtonian fluid models subject to various configurations remains a topic of great interest for researchers due to the wide range of applications. Owing to such importance, various examinations were accomplished by investigators to study non-Newtonian fluid flows. Recently, Manvi et al. [1] offered study on Eyring-Powell fluid flow in the presence of magnetic field and heat dissipation effects. Runge-Kutta (RK)-scheme was used for solution outcomes. It was demonstrated that raising the stratification parameter decreases velocity as well as temperature, and the opposite in the case for heat generation. Shahzad et al. [2] investigated natural convection energy transmission in a trapezoidal enclosure using coupled buoyancy effects of stratification. The Casson fluid rheological constitutive model, which depicts the properties of viscoelastic liquids, was envisioned. The impact of the slanted magnetic field, which is regulated by the Lorentz field law, was also addressed. The finite element approach was used to depict solution. Heat flux, kinetic energy, and mass flux were displayed graphically and tabulated. Pasha et al. [3] modelled and numerically simulated the non-Newtonian fluid having shear-thickening characteristics. The fluid was equipped in a hexagonal domain along with magnetic field and alumina nanoparticles. The finite element approach was used to discretize the equations system that resulted from the mathematical modeling of the physical situation. The results showed that increasing the strength-law index from 1.2 to 1.8 and the magnetic field's strength from 0 to 80 will decrease the mean Nusselt by 12.1% and 27.5%. The advancement in this direction can be accessed in Refs. [4−7].

The tangent hyperbolic fluid flow model is regarded as the most relevant liquid model in the class of non-Newtonian liquids in the context of numerous industrial applications such as porous industrial

materials, polymer solutions, oil recovery, ceramic processing, and fluid beds. From an experimental standpoint, it is seen that the tangent hyperbolic flow model accurately predicts shear thinning behavior. It is frequently utilized in laboratory research, medicine, and engineering fields for a variety of applications such as blood, polymers, paints, and melt investigations. Aside from that, the fluid model under consideration is of the rate type, and it exhibits relaxation and retardation time characteristics.

Owing to such importance, various researchers considered examination of tangent hyperbolic fluid flow, like the influence of heat and mass transfer on peristaltic flow of a tangent hyperbolic fluid (THF) in an annulus, which was investigated by Akbar et al. [8]. By assuming a long wavelength and low Reynolds number, the flow equations of THF were simplified. For the heat and concentration fields, exact solutions were evaluated, whereas the velocity profile was solved analytically and numerically. A graph and table were used to compare the two solutions. For various embedded parameters, temperature, pressure rise, concentration field, and pressure gradient were drafted and analyzed.

The impact of nanoparticles for THF with magnetohydrodynamics (MHD) was investigated by Akram and Nadeem [9]. Under the lubrication approach, the flow equations of a nanofluid were executed. Using a homotopy perturbation technique, the coupled temperature equation and nanoparticle volume fraction were solved analytically. The perturbation technique was used to solve the stream function and pressure gradient analytically. The graphical findings of the problem under investigation were also taken into account to observe the behavior of various physical parameters.

Naseer et al. [10] investigated the THF moving in the axial direction across a vertical exponentially extending cylinder with heat transfer. The flow equations were obtained by applying the normal boundary layer with a sufficient similarity transformation to the specified PDEs and boundary conditions. The RK-Fehlberg technique was used to solve this system of ordinary differential equations with boundary conditions. The graphs depicted the impacts of the related parameters, such as Weissenberg numbers, Reynolds numbers, Prandtl numbers, and the natural convection parameter. The skin friction coefficient and Nusselt numbers were presented as the corresponding physical attributes of the flow and heat transfer characteristics.

Gaffar et al. [11] studied the nonlinear THF over a sphere. Using the Keller Box technique, the altered conservation equations were numerically solved subject to physically suitable boundary conditions. The effects of several developing characteristics on flow field were thoroughly investigated. Additionally, the impacts of these parameters on heat transfer rate and skin friction were studied. It was discovered that when the Weissenberg number climbed, skin friction, the velocity, and the Nusselt number dropped.

The magnetic peristaltic flow TH nanofluid in an inclined tube with flexible walls was investigated by Hayat et al. [12]. In the problem definition, a nanofluid with Brownian motion and thermophoresis effects were used. There was thermal radiation and Joule heating. The formulation was finalized by taking into account slide circumstances in terms of temperature, velocity, and concentration. The lubrication approach was used to generate the problem formulation. The significance of several associated parameters on the flow was illustrated. The slip effect increases velocity and temperature while decreasing concentration. Thermal radiation reduced temperature, whereas bigger Hartman numbers increased temperature in response to the Joule heating effect.

Hayat et al. [13] investigated the nonlinear thermal radiation behavior of TH nanofluid via stretched surface. The flow analysis was presented while taking into account the chemical reaction and heat generation/absorption effects. To analyze heat and mass transmission, convective-type conditions were imposed. Because of the consideration of thermophoresis and Brownian motion, nanoparticle effects were seen. By using similarity transformations, the governing nonlinear partial differential systems were transformed into nonlinear ordinary differential systems. For temperature, velocity, and

concentration, the series solutions converged. The variations in temperature, velocity, and concentration distributions were investigated.

Rehman et al. [14] communicated numerically the THF flow yields of both cylindrical and flat surfaces. They assumed tangent hyperbolic fluid flow towards an inclined surface and obtained fluid flow by allowing no-slip conditions. Furthermore, momentum equations recognize magnetic field and mixed convection effects, whereas heat equations recognize the roles of thermal stratification and thermal radiation. The entire physical situation was translated into partial differential equations (PDEs), and a computational approach was used to solve it. The acquired results were presented in both graphical and tabular formats. In addition, a straight line of investigation was carried out to investigate the impact of mixed convection, an inclination impact on skin friction.

Kumar et al. [15] presented a numerical investigation of the compressed flow of THF toward sensor surface with varying thermal conductivity. The controlling equations were reassembled into conventional non-linear differential equations using appropriate transformation, and the resulting equations were numerically solved using the RKF45 technique. The effects of the impartment parameter on the flow field were depicted graphically. Variations in the flow index, Weissenberg number, and parameter of permeable velocity were discovered to have a considerable influence on the thermal and momentum boundary layer thickness.

Nagendramma et al. [16] investigated THF towards a cylinder with sink and heat source effects in porous space beneath nanoparticles. Brownian and thermophoretic mobility were taken into account when developing the mathematical model of TH-nanofluid. The equations were solved by using the RK scheme. The effects of parameters were visually depicted, and engineering-interest physical characteristics such as Nusselt, skin friction, and Sherwood number were investigated numerically. Momentum thickness increases for curvature and power-law index.

Heat and mass transmission of magnetohydrodynamics (MHD) TH-nanofluid were investigated by Atif et al. [17]. On its route, the nanofluid flow was believed to be directed by a wedge. The PDEs were converted into a nonlinear ordinary differential equations (ODEs) set. The well-known shooting method was used to solve the ensuing ODEs for two separate cases: namely, stretched and static wedge. The effect of complex physical factors on flow profiles was visually studied. The escalating Biot number, Brownian motion parameter, and thermophoresis parameter were discovered. The recent developments in examination of the tangent hyperbolic fluid can be assessed in Refs. [18−22].

Motivated by the literature reported above, we have offered the neural networking analysis on THF flow towards a magnetized surface. The heat and mass transfer aspects are considered in the presence of heat generation, velocity slip, and temperature slip effects. The flow is modelled in terms of PDEs and the Lie symmetry approach is used to construct the Lie group of transformation. Such transformations are used to reduce the order of PDEs. The shooting method is used to report the outcomes. An artificial neural network model is constructed to make predictions for the skin friction coefficient at the magnetized surface. To train the network, Levenberg-Marquardt backpropagation is utilized. Mean square error and regression analysis are both utilized to evaluate the performance of the constructed neural network model. The key novelty of the present article includes:

- Construction of neural network model to predict the impact of power law index and Weissenberg number on skin friction coefficient (SFC).
- Impact of power law index and velocity slip on tangent hyperbolic fluid flow field.
- Relation of magnetic field parameter on the flow field.
- Impact of Weissenberg number on the velocity of the tangent hyperbolic fluid.

2. Fluid flow formulation

The tangent hyperbolic fluid flow is considered over a flat surface. Aspects of both heat and mass transmission are considered. The uniform magnetic field is applied perpendicular to the flow. The novelty is enhanced by taking the heat generation effect by means of the energy equation. The strength of concentration and temperature near the surface is greater than the strength further away from the surface. The viscous dissipation effects are ignored while velocity and temperature slips are owned. The flow field can be formulated as follows [18,23]:

$$U_X + V_Y = 0, \tag{1}$$

$$UU_X + VU_Y = \nu_1 U_{YY}(1-m) + \sqrt{2}\,\Gamma U_Y U_{YY} \nu_1 m - (\sigma B^2/\rho)U, \tag{2}$$

$$UT_X + VT_Y = (k/c_p\rho)T_{YY} + (Q_1/c_p\rho)(T - T_\infty), \tag{3}$$

$$UC_X + VC_Y = D_c C_{YY}, \tag{4}$$

considering velocity and thermal slip, we reached at

$$U = bX + L_1 U_Y,\ V = 0,\ T = T_w + D_1 T_Y,\ \ C = C_w \ \text{ for } Y = 0,$$

$$U \to 0,\ T \to T_\infty,\ C \to C_\infty, \text{ when } Y \to \infty. \tag{5}$$

By considering:

$$\phi_{con} = \frac{C - C_\infty}{C_w - C_\infty},\ \theta_{tem} = \frac{T - T_\infty}{T_w - T_\infty},\ v = \frac{V}{\sqrt{b\nu_1}},\ u = \frac{U}{\sqrt{b\nu_1}},\ y = \sqrt{\frac{b}{\nu_1}}\,Y,\ \ x = \sqrt{\frac{b}{\nu_1}}\,X, \tag{6}$$

by plugging Eq (6) into the Eqs (1)−(5), we get the following forms:

$$u_x + v_y = 0, \tag{7}$$

$$uu_x + vu_y = u_{yy}(1-m) + \sqrt{2}\ \Gamma u_y u_{yy} bm - (\sigma B^2/\rho b)u, \tag{8}$$

$$u\theta_{tem,x} + v\theta_{tem,y} = (k/c_p\mu)\theta_{tem,yy} + (Q_1/c_p\rho b)\theta_{tem}, \tag{9}$$

$$u\phi_{con,x} + v\phi_{con,y} = (D_c/\nu_1)\phi_{con,yy}, \tag{10}$$

and

$$u = x + \sqrt{\frac{b}{\nu_1}}L_1 u_y,\ v = 0,\ \theta_{tem} = 1 + \sqrt{\frac{b}{\nu_1}}D_1\,\theta_{tem,y},\ \ \phi_{con} = 1 \ \text{ for } y = 0,$$

$$u \to 0,\ \theta_{tem} \to 0,\ \phi_{con} \to 0, \text{ when } y \to \infty. \tag{11}$$

Further, by using a stream function:

$$u = \Psi_y, v = -\Psi_x, \tag{12}$$

the use of Eq (12) into Eqs (7)−(11) results the following forms:

$$\Psi_{xy} - \Psi_{yx} = 0, \tag{13}$$

$$\Psi_y \Psi_{xy} - \Psi_x \Psi_{yy} = \Psi_{yyy}(1-m) + \sqrt{2}\,\Gamma \Psi_{yy} \Psi_{yyy} b\,m - (\sigma B^2 / \rho b)\Psi_y, \tag{14}$$

$$\Psi_y\, \theta_{tem,x} - \Psi_x\, \theta_{tem,y} = (k / c_p \mu)\theta_{tem,yy} + (Q_1 / c_p \rho b)\theta_{tem}, \tag{15}$$

$$\Psi_y\ \phi_{con,x} - \Psi_x \phi_{con,y} = (D_c / \nu_1)\phi_{con,yy}, \tag{16}$$

and

$$\Psi_y = x + \sqrt{\frac{b}{\nu_1}} L_1 \Psi_{yy},\ \Psi_x = 0,\ \theta_{tem} = 1 + \sqrt{\frac{b}{\nu_1}} D_1\, \theta_{tem,y},\ \ \phi_{con} = 1 \ \text{ for } y = 0,$$

$$\Psi_y \to 0,\ \theta_{tem} \to 0,\ \phi_{con} \to 0, \text{ when } \ y \to \infty. \tag{17}$$

3. Group theoretic examination

Our interest is to get an equivalent system subject to flow equations given as Eqs (8)−(10). The most common practice in this regard is to use some suitable set of transformations [24−26]. For a better description of the problem, we will construct the relevant transformation by using the Lie symmetry approach instead of choosing a random set of transformations. Therefore, consider the following set of transformations:

$$\Pi_1:\ X_1 = x e^{\varepsilon A_1},\ Y_1 = y e^{\varepsilon A_2},\ \Psi^* = \Psi e^{\varepsilon A_3},\ \theta_{tem}{}^* = \theta_{tem} e^{\varepsilon A_4}, \Gamma^* = \Gamma e^{\varepsilon A_5}, \phi_{con}{}^* = \phi_{con} e^{\varepsilon A_6}. \tag{18}$$

Here, coordinates $(\phi_{con}, \theta_{tem}, \Gamma, \Psi, y, x)$ are transformed as $(\phi_{con}{}^*, \theta_{tem}{}^*, \Gamma^*, \Psi^*, Y_1, X_1)$ by following Eq (18). Therefore, we have

$$\begin{aligned} &e^{\varepsilon(A_1+2A_2-2A_3)}\left(\Psi^*_{Y_1}\,\Psi^*_{X_1Y_1} - \Psi^*_{X_1}\,\Psi^*_{Y_1Y_1}\right) = e^{\varepsilon(3A_2-A_3)}\Psi^*_{Y_1Y_1Y_1}(1-m) \\ &+e^{\varepsilon(5A_2-2A_3-A_5)}\sqrt{2}\ \Gamma^*\Psi^*_{Y_1Y_1}\,\Psi^*_{Y_1Y_1Y_1}\,b\,m - e^{\varepsilon(A_2-A_3)}(\sigma B^2/\rho b)\Psi^*_{Y_1}, \end{aligned} \tag{19}$$

$$\begin{aligned} &e^{\varepsilon(A_1+A_2-A_3-A_4)}\left(\Psi^*_{Y_1}\,\theta_{tem}{}^*_{X_1} - \Psi^*_{X_1}\,\theta_{tem}{}^*_{Y_1}\right) = e^{\varepsilon(2A_2-A_4)}(k/c_p\mu)\,\theta_{tem}{}^*_{Y_1Y_1} \\ &+e^{-\varepsilon A_4}(Q_1/c_p\rho b)\theta_{tem}{}^*, \end{aligned} \tag{20}$$

$$e^{\varepsilon(A_1+A_2-A_3-A_6)}\left(\Psi^*_{Y_1}\,\phi^*_{X_1} - \Psi^*_{X_1}\,\phi^*_{Y_1}\right) = e^{\varepsilon(2A_2-A_6)}(D_c/\nu_1)\phi^*_{Y_1Y_1}. \tag{21}$$

Equations (19)−(21) admitted the preservation under scaling transformation Π_1, with relation

$$A_1+2A_2-2A_3=3A_2-A_3=5A_2-2A_3-A_5=A_2-A_3,$$

$$A_1+A_2-A_3-A_4=2A_2-A_4=-A_4, \tag{22}$$

$$A_1+A_2-A_3-A_6=2A_2-A_6.$$

The boundary conditions refer to the conclusion $A_4=0,$ and $A_6=0.$ The solution of Eq (22) refers to

$$A_1=A_1,\ A_2=0,\ A_3=A_1,\ A_4=0,\ A_5=-A_1 \text{ and } A_6=0. \tag{23}$$

The one parameter group of transformation reaches

$$\Pi_1:\ X_1=xe^{\varepsilon A_1},\ Y_1=y,\ \Psi^*=\Psi e^{\varepsilon A_1},\ \theta_{tem}{}^*=\theta_{tem},\ \Gamma^*=\Gamma e^{-\varepsilon A_1},\ \phi_{con}{}^*=\phi_{con}. \tag{24}$$

For Π_1 and around $\varepsilon=0$ up to order $O(\varepsilon)$, Taylors expansion results in

$$\Pi_1:\ X_1-x=x\varepsilon A_1+O(\varepsilon),\ Y_1-y=0+O(\varepsilon),\ \Psi^*-\Psi=x\varepsilon A_1+O(\varepsilon),$$

$$\theta_{tem}{}^*-\theta_{tem}=0+O(\varepsilon),\Gamma^*-\Gamma=-x\varepsilon A_1+O(\varepsilon),\ \phi_{con}{}^*-\phi_{con}=0+O(\varepsilon). \tag{25}$$

Owing to Eq (25), the characteristic equation becomes

$$\frac{dx}{xA_1}=\frac{dy}{0}=\frac{d\Psi}{xA_1}=\frac{d\theta_{tem}}{0}=\frac{d\Gamma}{-xA_1}=\frac{d\phi_{con}}{0}. \tag{26}$$

The possible combination results in

$$\chi=y,\ \Psi=xF(\chi),\ \theta_{tem}=\theta_{tem}(\chi),\ \Gamma=x^{-1}\Gamma_0,\ \phi_{con}=\phi_{con}(\chi). \tag{27}$$

Therefore, the Eqs (14)−(17) reduce to

$$\frac{d^3F(\chi)}{d\chi^3}(1-m)-\left(\frac{dF(\chi)}{d\chi}\right)^2+\frac{d^2F(\chi)}{d\chi^2}F(\chi)+mW_n\frac{d^3F(\chi)}{d\chi^3}\frac{d^2F(\chi)}{d\chi^2}$$
$$-H_a{}^2\frac{dF(\chi)}{d\chi}=0, \tag{28}$$

$$\frac{d^2\theta_{tem}(\chi)}{d\chi^2}+\Pr\left(F(\chi)\frac{d\theta_{tem}(\chi)}{d\chi}+H^{\pm}\theta_{tem}(\chi)\right)=0, \tag{29}$$

$$\frac{d^2\phi_{con}(\chi)}{d\chi^2}+Sc\left(F(\chi)\frac{d\phi_{con}(\chi)}{d\chi}\right)=0, \tag{30}$$

and boundary conditions (BCs) are

$$F(\chi)=0,\frac{dF(\chi)}{d\chi}=1+\beta_1\frac{d^2F(\chi)}{d\chi^2},\ \theta_{tem}(\chi)=1+\beta_2\frac{d\theta_{tem}(\chi)}{d\chi},\ \phi_{con}(\chi)=1\ \text{at}\ \chi=0,$$
$$\frac{dF(\chi)}{d\chi}\to 0,\ \theta_{tem}(\chi)\to 0,\ \phi_{con}(\chi)\to 0,\ \text{when}\ \ \chi\to\infty. \tag{31}$$

Since we have considered flow over a flat surface, skin friction coefficient will play the role of an important engineering quantity. We will evaluate the SFC in terms of important flow parameters. The mathematical relation is as follows:

$$C_F=\frac{\Delta_w}{\rho(bx)^2},\ \text{and}\,\Delta_w=(1-m)u_y+\frac{m\Gamma}{\sqrt{2}}(u_y)^2, \tag{32}$$

while the concluded mathematical relation can be written as follows:

$$SFC=(1-m)\frac{d^2F(0)}{d\chi^2}+(m/2)W_n\left[\frac{d^2F(0)}{d\chi^2}\right]^2. \tag{33}$$

The involved flow parameters are defined as:

$$W_n=\sqrt{2}\Gamma_0 b,\ \ H_a=\sqrt{\frac{\sigma B^2}{\rho b}},\ \ \text{Pr}=\frac{\mu c_p}{k},$$
$$H^+=\frac{Q_1}{\rho c_p b},\ \ Sc=\frac{\nu_1}{D_c},\ \beta_1=\sqrt{\frac{b}{\nu_1}}L_1,\beta_2=\sqrt{\frac{b}{\nu_1}}D_1. \tag{34}$$

4. Numerical scheme

A non-Newtonian fluid model is mathematically modelled in terms of PDEs and later symmetry transformations are constructed to drop the order of PDEs. To describe the flow differential equations, several solution approaches [27−30] are employed, but we will use the shooting method [31−33] to find the best approximate numerical solution. To execute the solution scheme, the equivalent system is obtained in terms of first-order differential equations. Such outcomes are achieved by using the following suitable set of substitutions:

$$M_1=F(\chi),\ \ M_2=\frac{dF(\chi)}{d\chi},M_3=\frac{d^2F(\chi)}{d\chi^2},\ M_4=\theta_{tem}(\chi),$$
$$M_5=\frac{d\theta_{tem}(\chi)}{d\chi},M_6=\phi_{con}(\chi),\ M_7=\frac{d\phi_{con}(\chi)}{d\chi}, \tag{35}$$

and the reduced system of first order differential equations can be concluded to be:

$$\frac{dM_1(\chi)}{d\chi} = M_2(\chi), \frac{dM_2(\chi)}{d\chi} = M_3(\chi),$$
$$\frac{dM_3(\chi)}{d\chi} = \frac{\left(M_2(\chi)\right)^2 - M_3(\chi)M_1(\chi) + H_a{}^2 M_2(\chi)}{(1-m) + mW_n M_3(\chi)},$$
$$\frac{dM_4(\chi)}{d\chi} = M_5(\chi), \frac{dM_5(\chi)}{d\chi} = -\Pr\left(M_5(\chi)M_1(\chi) + H^+ M_4(\chi)\right),$$
$$\frac{dM_6(\chi)}{d\chi} = M_7(\chi), \frac{dM_7(\chi)}{d\chi} = -Sc\left(M_7(\chi)M_1(\chi)\right), \tag{36}$$

and conditions far away from the surface take the form

$$M_2(\chi) \to 0, M_4(\chi) \to 0, M_6(\chi) \to 0, \text{ at } \chi \to \infty. \tag{37}$$

5. Neural network analysis

The non-Newtonian fluid model is considered over a flat surface along with various physical effects, which include velocity slip, magnetic field, thermal slip, and heat generation. The fluid problem is mathematically modelled and Eqs (1)−(4) describe continuity, momentum, energy, and concentration equations, respectively.

Equation (5) remarks the endpoint condition along with velocity and temperature slip assumptions. Eq (6) is used to have dimensionless forms, namely, Eqs (7)−(11) against Eqs (1)−(5). In terms of the stream function, Eqs (7)−(11) take the form of Eqs (13)−(17). It is common practice for researchers affiliated with fluid science to transform the PDEs into equivalent systems of ODEs. This can be done by using a suitable set of transformations. Such transformation can be picked from literature randomly, but for a better description of the problem, we construct the set of transformations for our flow problem by using Lie symmetry analysis. The necessary procedure in this regard is debated from Eq (18) to Eq (27). Equation (27) describes the set of transformations that are used to step down the order of flow narrating PDEs. Equations (28)−(30) are the ultimate flow narrating boundary value problem (BVP) that can be used to examine the THF over a flat surface.

The key flow-affecting parameters are the power law index, Schmidt number, Prandtl number, Weissenberg number, heat generation, magnetic field, velocity slip, and temperature slip parameters. Our interest is to examine the effect of the power law index and Weissenberg number on SFC for both frames, namely, magnetic and non-magnetic. Tables 1−4 are evidence in this direction. In detail, Table 1 offers the numerical outcomes of SFC towards power law index when an externally applied magnetic field is neglected. In an absolute sense, one can see that when we increase the power law index, the SFC reduces significantly. Table 2 gives the numerical outcomes of SFC towards the power law index when an externally applied magnetic field is considered. We can see that the SFC admits an inverse relation towards positive variation in *m*. One can see that the strength of SFC is slightly higher for the magnetized surface. Table 3 shows the variation in SFC towards higher values of W_n.

Table 1. Impact of power law index on SFC for the non-magnetic case.

m	$F''(0)$	$SFC = (1-m)\frac{d^2F(0)}{d\chi^2} + (m/2)W_n\left[\frac{d^2F(0)}{d\chi^2}\right]^2$
0.10	−0.9160	−0.82020472
0.15	−0.9406	−0.792874537
0.30	−1.0301	−0.70515341
0.35	−1.0670	−0.673626443
0.45	−1.1567	−0.606081015
0.50	−1.2125	−0.569496094
0.55	−1.2791	−0.530602338
0.60	−1.3609	−0.488798536
0.65	−1.4655	−0.443125067
0.70	−1.6089	−0.392070428
0.75	−1.8337	−0.332332912
0.80	−2.4339	−0.249825232

Table 2. Impact of power law index on SFC for the magnetic case.

m	$F''(0)$	$SFC = (1-m)\frac{d^2F(0)}{d\chi^2} + (m/2)W_n\left[\frac{d^2F(0)}{d\chi^2}\right]^2$
0.10	−0.9204	−0.824124319
0.15	−0.9451	−0.796635895
0.30	−1.0350	−0.708431625
0.35	−1.0721	−0.676750528
0.45	−1.1623	−0.608868821
0.50	−1.2185	−0.572131444
0.55	−1.2855	−0.533030968
0.60	−1.3677	−0.490961901
0.65	−1.4730	−0.445033808
0.70	−1.6175	−0.393679281
0.75	−1.8445	−0.333543241
0.80	−2.4646	−0.249949874

Table 3. Impact of Weissenberg number on SFC for the non-magnetic case.

W_n	$F''(0)$	$SFC = (1-m)\frac{d^2F(0)}{d\chi^2} + (m/2)W_n\left[\frac{d^2F(0)}{d\chi^2}\right]^2$
0.10	−0.916	−0.82020472
0.15	−0.9173	−0.819259205
0.30	−0.9213	−0.816438095
0.35	−0.9226	−0.815444162
0.45	−0.9253	−0.813505948
0.50	−0.9267	−0.812560678
0.55	−0.9281	−0.811602336
0.60	−0.9294	−0.810546469
0.65	−0.9299	−0.808806795
0.70	−0.9323	−0.808648585
0.75	−0.9337	−0.807637662
0.80	−0.9351	−0.80661352

Table 4. Impact of Weissenberg number on SFC for the magnetic case.

W_n	$F''(0)$	$SFC = (1-m)\frac{d^2F(0)}{d\chi^2} + (m/2)W_n\left[\frac{d^2F(0)}{d\chi^2}\right]^2$
0.10	−0.9333	−0.835614756
0.15	−0.9346	−0.834588921
0.30	−0.9387	−0.831612635
0.35	−0.9401	−0.83062371
0.45	−0.943	−0.828691898
0.50	−0.9444	−0.827662716
0.55	−0.9458	−0.826620215
0.60	−0.9473	−0.825648681
0.65	−0.9487	−0.82457897
0.70	−0.9502	−0.823579199
0.75	−0.9517	−0.822565017
0.80	−0.9532	−0.82153639

Following the absolute sense, we have seen that the SFC shows opposite trends, that is, increase in W_n causes a decline in SFC. Such observation is done for a non-magnetic surface. Table 4 provides the impact of W_n on SFC for a magnetic flat surface. For higher values of the Weissenberg number, the SFC shows a trivial change. Important to note that the SFC admits higher magnitude towards *m* for the case of a magnetized flat surface.

The prediction norm of artificial intelligence is a topic of great attention by researchers in every field. Particularly in the field of fluid science, use of AI is gaining much importance. The motivation in this regard can be accessed in Refs. [34,35]. Owing to such importance, we have constructed the neural network model [36−39] to study the variation in skin friction coefficient towards three different

flow parameters. Such a neural network model can be used to get the values of SFC up to a wide range of flow parameters where the actual solution method fails to determine said values. In detail, the power law index, Weissenberg number, and magnetic field parameter are considered three inputs to construct an artificial neural network (ANN) model to predict SFC. Ten neurons are considered in the hidden layer and the last layer holds SFC as an output. The neural network model is illustrated in Figure 1.

We have considered both magnetic and non-magnetic outcomes for the SFC coefficient and hence a total of 88 samples are considered for three inputs. For better training of the neural network model, the 88 samples are randomly chosen with a standard ratio of 70/30, as 62 (70%), 13 (15%), and 13 (15%) for training, validation, and testing, respectively. The 62 samples helped to train the network and it was adjusted by following the error. The network generalization is measured by using 15% of the data and 15% of the data is used for testing. The Levenberg-Marquardt backpropagation is used to train the network by considering the random 62 samples values out of 88. Both mean square error and regression analysis are used to check the performance of the developed neural network model. The relations are:

$$MSE = \frac{1}{N}\sum_{i=1}^{N}(X_{\text{num}(i)} - X_{\text{ANN}(i)})^2. \tag{38}$$

$$R = \sqrt{1 - \frac{\sum_{i=1}^{N}(X_{\text{num}(i)} - X_{\text{ANN}(i)})^2}{\sum_{i=1}^{N}(X_{\text{num}(i)})^2}}. \tag{39}$$

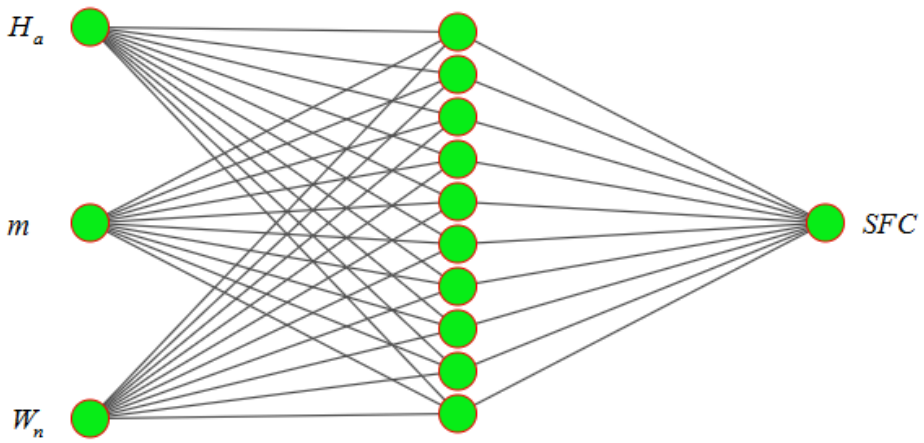

Figure 1. ANN model diagram.

Figure 2 offers the mean square error (MSE) plot for the ANN model to predict the SFC at a flat surface. Error is noticed up to 12 epochs. We have seen that MSE for training, validation, and testing is decreased significantly up to 2 epochs, and after that, it converges to a specific value for each scheme. Collectively, the best validation performance is 0.00060476 achieved at epoch 6. The error histogram of the developed model is given in Figure 3. It can be seen that the difference as an error between the targeted and predicted values of SFC is very small. The training of the ANN model is completed successfully.

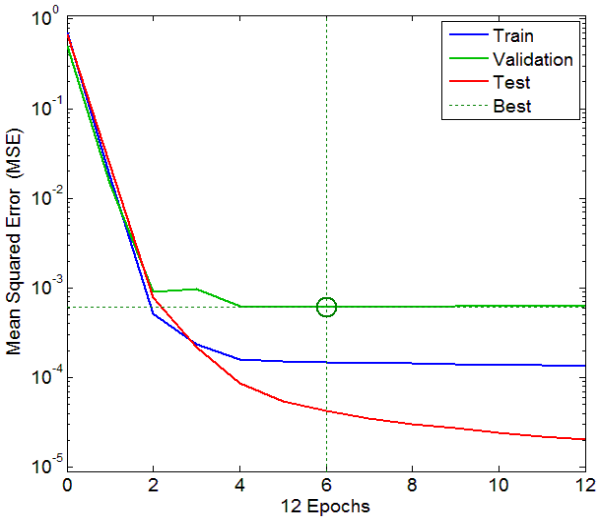

Figure 2. Performance plot of network.

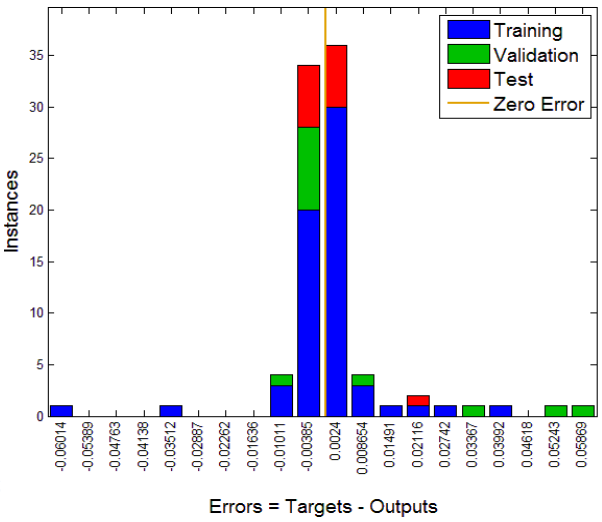

Figure 3. Histogram of ANN.

Figure 4 offers the regression plot for the training scheme of the ANN model and we have noticed R = 0.99767, which is quite close to R = 1. Therefore, the random values of the training phase possess a strong correlation. The MSE error subject to the training phase is MSE = 1.47895e^{-04} which is very low and hence the error between predicted and targeted values is very low. The constructed ANN model is best to predict the SFC at the surface manifested with heat generation and MHD effects. For validation, we observed R = 0.9899 and MSE = 6.0476e^{-04}. For the testing phase, we observed R = 0.9996 and MSE = 4.2304e^{-05}. Figure 5 provided the regression plot for all, namely testing, validation, and training. In this case, the coefficient of determination is R = 0.99688, which is close to R = 1, and hence the collected sample values of SFC for three inputs are strongly correlated. Figure 6 offers the error in terms of a bar graph.

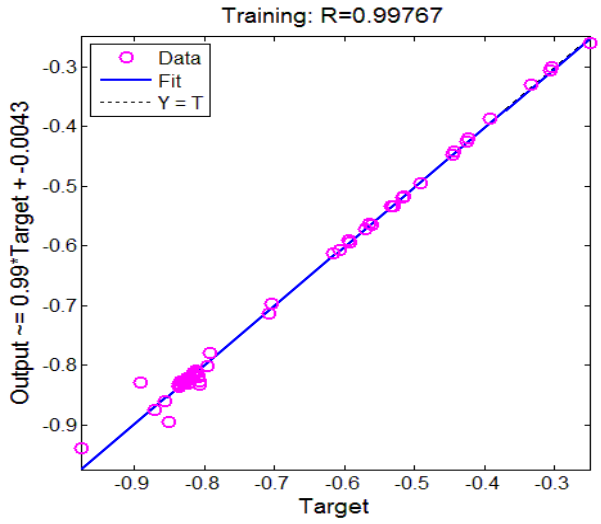

Figure 4. Training regression plot for ANN.

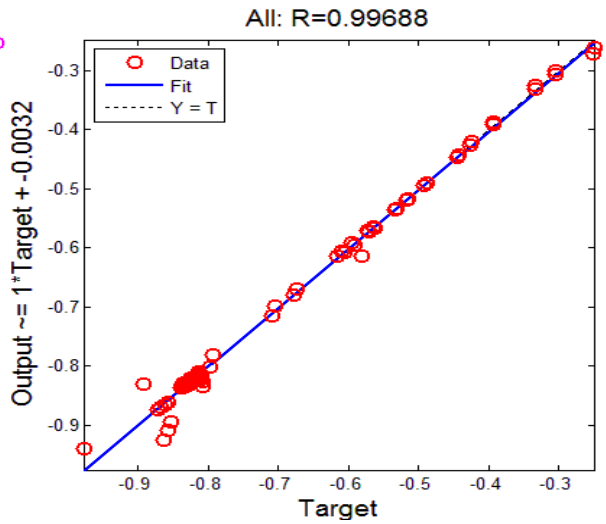

Figure 5. Regression plot for all (training, testing, and validation) of ANN.

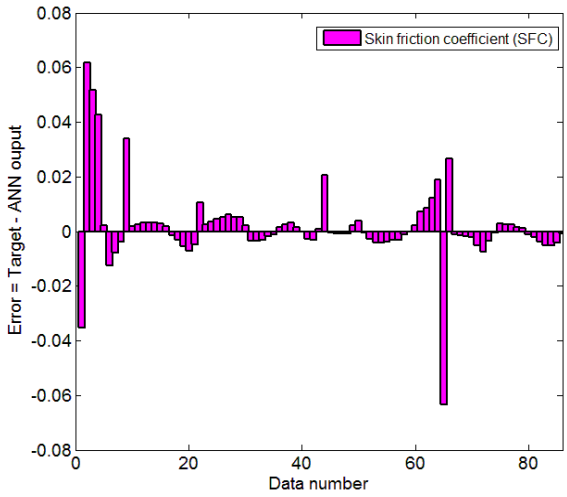

Figure 6. Error plot for ANN model.

We can see that the error between original values and predicted values is very low. Only two values out of 88 hold the error ± 0.06. Therefore, we can conclude that the constructed ANN is best to predict the values of SFC. Figure 7 offers a comparison of SFC targeted values and SFC predicted values by ANN model. We can see that the predicted values of SFC by the ANN are the same as the original values. The impacts of specific values of Weissenberg number, magnetic field parameter, power law index, and velocity slip parameters on velocity are examined. Figures 8−11 are evidence in this regard. In detail, Figure 8 offers the impact of H_a on velocity. The range adopted is $H_a = 0.0$, 0.4, 0.8, and 1.2. We can see that for higher values of H_a, the velocity shows decline values. Higher values of $H_a = 0.0$, 0.4, 0.8 and 1.2 increase the strength of the Lorentz force. The resistive nature of Lorentz force is the cause that slows down the movement of tangent hyperbolic fluid and as a result the velocity drops. It is important to note that $H_a = 0.0$ corresponds to the non-magnetized flow of fluid and for this case, the strength of velocity is higher in comparison with the magnetic case that is $H_a = 0.4, 0.8$ and 1.2. Figure 9 gives the impact of W_n on velocity and we have seen that for large values of $W_n = 0.1, 0.3, 0.6$ and 0.9, the velocity shows a significant decline.

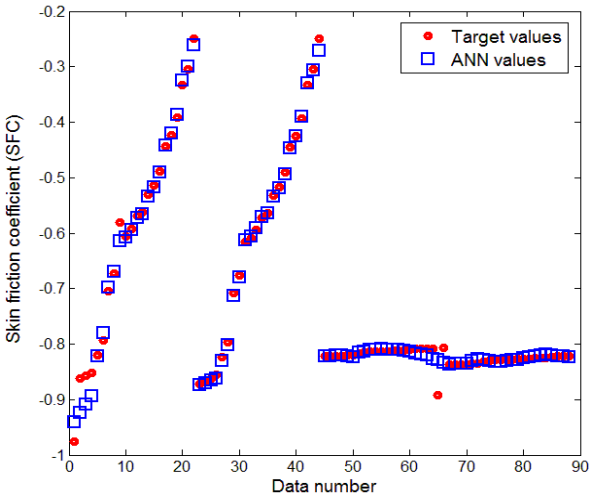

Figure 7. Results comparison for ANN model.

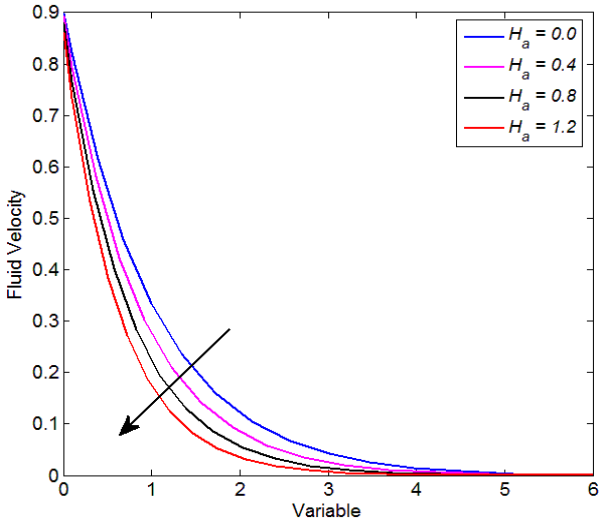

Figure 8. Effect of H_a on velocity.

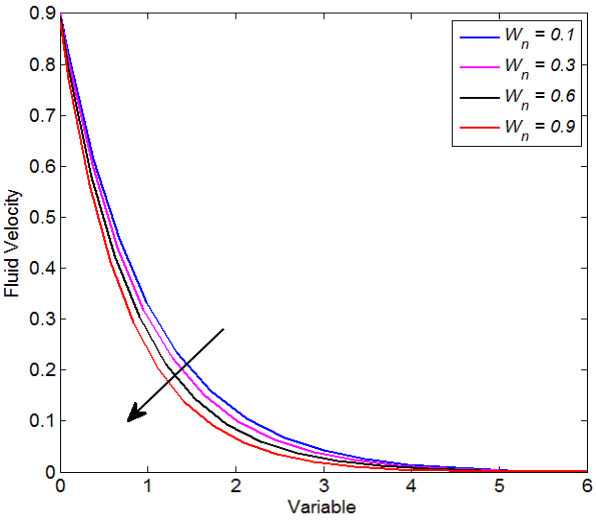

Figure 9. Effect of W_n on velocity.

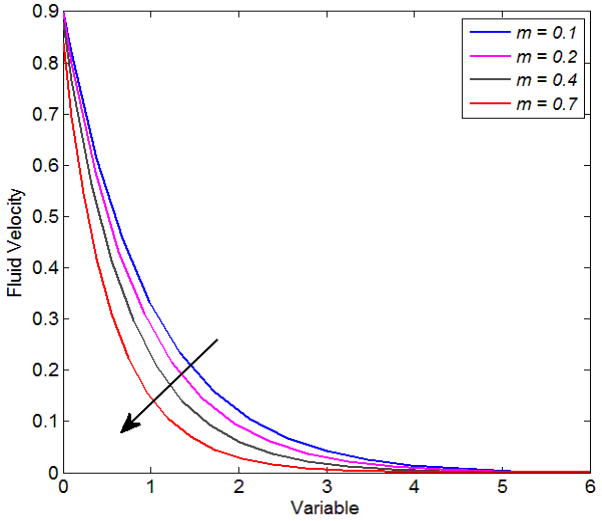

Figure 10. Effect of m on velocity.

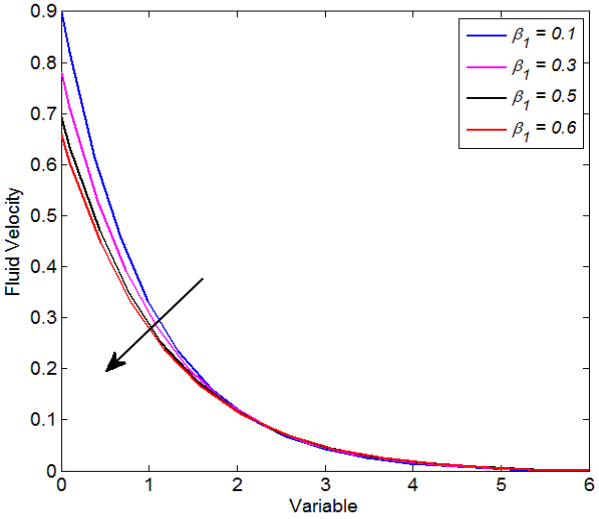

Figure 11. Effect of β_1 on velocity.

One can note that the larger the W_n, the greater the relaxation time. This brings resistance to fluid particles and consequences are concluded as a decline in fluid velocity. The impact of m on velocity is given in Figure 10. An inverse relation is observed for the present case. In detail, when we iterate the power law index m = 0.1, 0.2, 0.4, and 0.7, the velocity profile declines significantly. Higher values of the power law index enhance the fluid viscosity and hence fluid velocity drops. The effect of the velocity slip parameter on fluid velocity is inspected and the outcome is given in Figure 11. It is seen that positive variation in β_1 causes a decline in fluid velocity. Such decline is significant up-to an independent variable of range $0 \le \chi \le 1.5$.

Tables 5−8 are constructed to offer the comparison of numerical values of targeted values of SFC and predicted value of SFC towards various flow parameters. In detail, Table 5 gives the numerical comparison of targeted and predicted values of SFC for the power law index in the non-magnetic case. Table 6 offers the numerical comparison of targeted and predicted values of SFC for the power law index in the magnetic case. In both cases, we have observed that the predicted and targeted values are

in great agreement. Table 7 offers the numerical comparison of targeted and predicted values of SFC for changing Weissenberg number in the non-magnetic case while Table 8 offers the comparison of SFC against positive values of Weissenberg number with an externally applied magnetic field. For both cases, the prediction by the neural networking model is accurate with minimal error.

Table 5. Numerical comparison of targeted and predicted values of SFC for power law index in the non-magnetic case.

Data number	SFC Targeted Values	SFC Predicted Values	Error
1.	−0.975159395	−0.939824589	−0.035330
2.	−0.862310368	−0.924123521	0.061813
3.	−0.857178428	−0.908992999	0.051815
4.	−0.851955002	−0.894491042	0.042536
5.	−0.82020472	−0.822297614	0.002093
6.	−0.792874537	−0.780406424	−0.012470
7.	−0.70515341	−0.697240748	−0.007910
8.	−0.673626443	−0.669805633	−0.003820
9.	−0.580676442	−0.614523469	0.033847
10.	−0.606081015	−0.607853943	0.001773
11.	−0.591681962	−0.594160273	0.002478
12.	−0.569496094	−0.572659458	0.003163
13.	−0.56194131	−0.56521336	0.003272
14.	−0.530602338	−0.533850544	0.003248
15.	−0.514284548	−0.517114385	0.002830
16.	−0.488798536	−0.490507447	0.001709
17.	−0.443125067	−0.441618766	−0.001510
18.	−0.423471145	−0.420316827	−0.003150
19.	−0.392070428	−0.386417913	−0.005650
20.	−0.332332912	−0.325155673	−0.007180
21.	−0.304184957	−0.299420599	−0.004760
22.	−0.249825232	−0.260386191	0.010561

Table 6. Numerical comparison of targeted and predicted values of SFC for power law index in the magnetic case.

Data number	SFC Targeted Values	SFC Predicted Values	Error
1.	−0.871604096	−0.874182807	0.002579
2.	−0.866418952	−0.87001473	0.003596
3.	−0.861241252	−0.865660607	0.004419
4.	−0.85597203	−0.861118228	0.005146
5.	−0.824124319	−0.830289686	0.006165
6.	−0.796635895	−0.80183647	0.005201
7.	−0.708431625	−0.713564716	0.005133
8.	−0.676750528	−0.678870995	0.002120

Continued on next page

Data number	SFC Targeted Values	SFC Predicted Values	Error
9.	−0.615974643	−0.612554215	−0.003420
10.	−0.608868821	−0.605378334	−0.003490
11.	−0.594434076	−0.591216526	−0.003220
12.	−0.572131444	−0.570244239	−0.001890
13.	−0.564505572	−0.563239627	−0.001270
14.	−0.533030968	−0.534382478	0.001352
15.	−0.516593100	−0.519008397	0.002415
16.	−0.490961901	−0.494102616	0.003141
17.	−0.445033808	−0.446377981	0.001344
18.	−0.425273212	−0.424985181	−0.00029
19.	−0.393679281	−0.390756647	−0.002920
20.	−0.333543241	−0.33029372	−0.003250
21.	−0.305182392	−0.305994817	0.000812
22.	−0.249949874	−0.270695122	0.020745

Table 7. Numerical comparison of targeted and predicted values of SFC for Weissenberg number in the non-magnetic case.

Data number	SFC Targeted Values	SFC Predicted Values	Error
1.	−0.821912576	−0.821407181	−0.00051
2.	−0.821764604	−0.820952634	−0.00081
3.	−0.821526358	−0.82072097	−0.00081
4.	−0.82137738	−0.820675089	−0.00070
5.	−0.82020472	−0.822297614	0.002093
6.	−0.819259205	−0.823155993	0.003897
7.	−0.816438095	−0.815776886	−0.00066
8.	−0.815444162	−0.812652845	−0.00279
9.	−0.81367625	−0.809374493	−0.00430
10.	−0.813505948	−0.809236058	−0.00427
11.	−0.813078017	−0.809098176	−0.00398
12.	−0.812560678	−0.809235384	−0.00333
13.	−0.812387111	−0.80937178	−0.00302
14.	−0.811602336	−0.810365938	−0.00124
15.	−0.811164508	−0.811132728	−3.2E-05
16.	−0.810546469	−0.812627386	0.002081
17.	−0.808806795	−0.816080535	0.007274
18.	−0.80919855	−0.817813692	0.008615
19.	−0.808648585	−0.820792271	0.012144
20.	−0.807637662	−0.826648602	0.019011
21.	−0.89247238	−0.829205126	−0.06327
22.	−0.80661352	−0.833084047	0.026471

Table 8. Numerical comparison of targeted and predicted values of SFC for Weissenberg number in the magnetic case.

Data number	SFC Targeted Values	SFC Predicted Values	Error
1.	−0.837376713	−0.83612492	−0.00125
2.	−0.837212867	−0.835695112	−0.00152
3.	−0.836958741	−0.835190128	−0.00177
4.	−0.83679387	−0.834616523	−0.00218
5.	−0.835614756	−0.830289686	−0.00533
6.	−0.834588921	−0.826935744	−0.00765
7.	−0.831612635	−0.827937662	−0.00367
8.	−0.83062371	−0.830234239	−0.00039
9.	−0.828878968	−0.831558496	0.002680
10.	−0.828691898	−0.831347166	0.002655
11.	−0.828230482	−0.830691406	0.002461
12.	−0.827662716	−0.829164862	0.001502
13.	−0.827472319	−0.8285303	0.001058
14.	−0.826620215	−0.825570143	−0.00105
15.	−0.826233321	−0.823983418	−0.00225
16.	−0.825648681	−0.821750637	−0.00390
17.	−0.82457897	−0.819293612	−0.00529
18.	−0.824348067	−0.818998991	−0.00535
19.	−0.823579199	−0.819387932	−0.00419
20.	−0.822565017	−0.82162853	−0.00094
21.	−0.822155301	−0.822581709	0.000426
22.	−0.82153639	−0.823280058	0.001744

In the absence of heat transfer, mass transfer, and considering $m = 0, W_n = 0$, our problem is reduced to that of Fathizadeh et al. [40]. Furthermore, the comparison is constructed with other available methods, namely the modified homotopy perturbation method (MHPM), homotopy perturbation method (HPM), and exact solution for various values of H_a. We found an excellent match (see Table 9), which supports the validity of the present work.

Table 9. Comparison with existing literature [40].

H_a	SFC			
	Present results	Exact solution	HPM	MHPM
0.0	−1.0000	−1.0000	−1.0000	−1.0000
1.0	−1.4140	−1.4142	−1.4142	−1.4142
5.0	−2.4493	−2.4494	−2.4494	−2.4494
10	−3.3167	−3.3166	−3.3166	−3.3166
50	−7.1415	−7.1414	−7.1414	−7.1414

6. Conclusions

Artificial intelligence-based analysis is performed to examine the magnetized THF flow towards the surface manifested with both velocity and thermal slip effects. The heat generation effect is added to the energy equation and mass transfer aspects are owned by means of the concentration equation. Lie transformations are used to step down the PDEs into ODEs and the shooting method is used to evaluate the flow field. SFC is evaluated by establishing a neural network model. By following neural analysis, the outcomes are as follows:

1) Owing to the training of the neural network, the best validation performance is 0.00060476, achieved at epoch 6. The MSE error subject to training, validation, and testing phases is MSE = $1.47895e^{-04}$, MSE = $6.0476e^{-04}$, and MSE = $4.2304e^{-05}$, respectively. The said values are quite low and appreciable.

2) The value of the coefficient of determination for all (training, validation, and testing) is R = 0.99688, which is close to R = 1 and hence the collected sample values of SFC for Weissenberg number, magnetic field parameter, and power law index are strongly correlated.

3) The SFC predicted values using a neural network model for Weissenberg number and power law index are matched with original values.

4) Owing to a prediction by ANN, for positive variation in both Weissenberg number and power law index, the magnitude of SFC is greater for a magnetized surface.

5) The velocity of fluid shows declining trends relative to the Weissenberg number, magnetic field parameter, velocity slip parameter, and power law index.

6) We are confident that the present neural findings will be helpful for researchers to best evaluate the fluid flow problems with engineering standpoints.

Use of AI tools declaration

The authors declare they have not used Artificial Intelligence (AI) tools in the creation of this article.

Acknowledgments

The authors would like to thank Prince Sultan University, Saudi Arabia, for the technical support through the TAS research lab.

Conflict of interest

The authors declare no conflict of interest.

References

1. B. Manvi, J. Tawade, M. Biradar, S. Noeiaghdam, U. Fernandez-Gamiz, V. Govindan, The effects of MHD radiating and non-uniform heat source/sink with heating on the momentum and heat transfer of Eyring-Powell fluid over a stretching, *Results Eng.*, **14** (2022), 100435. https://doi.org/10.1016/j.rineng.2022.100435
2. H. Shahzad, Q. U. Ain, A. A. Pasha, K. Irshad, I. A. Shah, A. Ghaffari, et al., Double-diffusive natural convection energy transfer in magnetically influenced Casson fluid flow in trapezoidal enclosure with fillets, *Int. Commun. Heat Mass*, **137** (2022), 106236. https://doi.org/10.1016/j.icheatmasstransfer.2022.106236

3. A. A. Pasha, M. M. Alam, T. Tayebi, S. Kasim, A. S. Dogonchi, K. Irshad, et al., Heat transfer and irreversibility evaluation of non-Newtonian nanofluid density-driven convection within a hexagonal-shaped domain influenced by an inclined magnetic field, *Case Stud. Therm. Eng.*, **41** (2023), 102588. https://doi.org/10.1016/j.csite.2022.102588
4. C. N. Guled, J. V. Tawade, P. Kumam, S. Noeiaghdam, I. Maharudrappa, S. M. Chithra, et al., The heat transfer effects of MHD slip flow with suction and injection and radiation over a shrinking sheet by optimal homotopy analysis method, *Results Eng.*, **18** (2023), 101173. https://doi.org/10.1016/j.rineng.2023.101173
5. G. Dharmaiah, J. L. R. Prasad, K. S. Balamurugan, I. Nurhidayat, U. Fernandez-Gamiz, S. Noeiaghdam, Performance of magnetic dipole contribution on ferromagnetic non-Newtonian radiative MHD blood flow: An application of biotechnology and medical sciences, *Heliyon*, **2** (2023). https://doi.org/10.1016/j.heliyon.2023.e13369
6. T. Sajid, W. Jamshed, M. R. Eid, S. Algarni, T. Alqahtani, R. W. Ibrahim, et al., Thermal case examination of inconstant heat source (sink) on viscous radiative sutterby nanofluid flowing via a penetrable rotative cone, *Case Stud. Therm. Eng.*, **48** (2023), 103102. https://doi.org/10.1016/j.csite.2023.103102
7. M. Waqas, Y. J. Xu, M. Nasir, M. M. Alam, A. A. Pasha, K. Irshad, et al., Darcy-Forchheimer mangetized flow based on differential type nanoliquid capturing Ohmic dissipation effects, *Propuls. Power Res.*, **12** (2023), 443−455. https://doi.org/10.1016/j.jppr.2023.08.003
8. N. S. Akbar, S. Nadeem, T. Hayat, A. A. Hendi, Effects of heat and mass transfer on the peristaltic flow of hyperbolic tangent fluid in an annulus, *Int. J. Heat Mass.*, **54** (2011), 4360−4369. https://doi.org/10.1016/j.ijheatmasstransfer.2011.03.064
9. S. Akram, S. Nadeem, Consequence of nanofluid on peristaltic transport of a hyperbolic tangent fluid model in the occurrence of apt (tending) magnetic field, *J. Magn. Magn. Mater.*, **358** (2014), 183−191. https://doi.org/10.1016/j.jmmm.2014.01.052
10. M. Naseer, M. Y. Malik, S. Nadeem, A. Rehman, The boundary layer flow of hyperbolic tangent fluid over a vertical exponentially stretching cylinder, *Alex. Eng. J.*, **53** (2014), 747−750. https://doi.org/10.1016/j.aej.2014.05.001
11. S. A. Gaffar, V. R. Prasad, O. A. Bég, Numerical study of flow and heat transfer of non-Newtonian tangent hyperbolic fluid from a sphere with Biot number effects, *Alex. Eng. J.*, **54** (2015), 829−841. https://doi.org/10.1016/j.aej.2015.07.001
12. T. Hayat, M. Shafique, A. Tanveer, A. Alsaedi, Magnetohydrodynamic effects on peristaltic flow of hyperbolic tangent nanofluid with slip conditions and Joule heating in an inclined channel, *Int. J. Heat Mass*, **102** (2016), 54−63. https://doi.org/10.1016/j.ijheatmasstransfer.2016.05.105
13. T. Hayat, S. Qayyum, A. Alsaedi, S. A. Shehzad, Nonlinear thermal radiation aspects in stagnation point flow of tangent hyperbolic nanofluid with double diffusive convection, *J. Mol. Liq.*, **223** (2016), 969−978. https://doi.org/10.1016/j.molliq.2016.08.102
14. K. U. Rehman, A. A. Malik, M. Y. Malik, N. U. Saba, Mutual effects of thermal radiations and thermal stratification on tangent hyperbolic fluid flow yields by both cylindrical and flat surfaces, *Case Stud. Therm. Eng.*, **10** (2017), 244−254. https://doi.org/10.1016/j.csite.2017.07.003
15. K. G. Kumar, B. J. Gireesha, M. R. Krishanamurthy, N. G. Rudraswamy, An unsteady squeezed flow of a tangent hyperbolic fluid over a sensor surface in the presence of variable thermal conductivity, *Results Phys.*, **7** (2017), 3031−3036. https://doi.org/10.1016/j.rinp.2017.08.021
16. V. Nagendramma, A. Leelarathnam, C. S. K. Raju, S. A. Shehzad, T. Hussain, Doubly stratified MHD tangent hyperbolic nanofluid flow due to permeable stretched cylinder, *Results Phys.*, **9** (2018), 23−32. https://doi.org/10.1016/j.rinp.2018.02.019

17. S. M. Atif, S. Hussain, M. Sagheer, Heat and mass transfer analysis of time-dependent tangent hyperbolic nanofluid flow past a wedge, *Phys. Lett. A*, **383** (2019), 1187−1198. https://doi.org/10.1016/j.physleta.2019.01.003
18. Z. Ullah, G. Zaman, A. Ishak, Magnetohydrodynamic tangent hyperbolic fluid flow past a stretching sheet, *Chinese J. Phys.*, **66** (2020), 258−268. https://doi.org/10.1016/j.cjph.2020.04.011
19. W. Khan, I. A. Badruddin, A. Ghaffari, H. M. Ali, Heat transfer in steady slip flow of tangent hyperbolic fluid over the lubricated surface of a stretchable rotatory disk, *Case Studi. Therm. Eng.*, **24** (2021), 100825. https://doi.org/10.1016/j.csite.2020.100825
20. S. Sindhu, B. J. Gireesha, Scrutinization of unsteady non-Newtonian fluid flow considering buoyancy effect and thermal radiation: Tangent hyperbolic model, *Int. Commun. Heat Mass*, **135** (2022), 106062. https://doi.org/10.1016/j.icheatmasstransfer.2022.106062
21. A. Hussain, N. Farooq, A. Ahmad, L. Sarwar, Impact of double diffusivity on the hyperbolic tangent model conveying nano fluid flow over the wedge, *Int. Commun. Heat Mass*, **145** (2023), 106849. https://doi.org/10.1016/j.icheatmasstransfer.2023.106849
22. M. A. Elogail, Peristaltic flow of a hyperbolic tangent fluid with variable parameters, *Results Eng.*, **17** (2023), 100955. https://doi.org/10.1016/j.rineng.2023.100955
23. N. S. Akbar, S. Nadeem, R. U. Haq, Z. H. Khan, Numerical solutions of magnetohydrodynamic boundary layer flow of tangent hyperbolic fluid towards a stretching sheet, *Indian J. Phys.*, **87** (2013), 1121−1124. https://doi.org/10.1007/s12648-013-0339-8
24. K. U. Rehman, N. U. Saba, M. Y. Malik, A. A. Malik, Encountering heat and mass transfer mechanisms simultaneously in Powell-Erying fluid through Lie symmetry approach, *Case Stud. Therm. Eng.*, **10** (2017), 541−549. https://doi.org/10.1016/j.csite.2017.10.011
25. K. U. Rehman, M. Y. Malik, I. Zehra, M. S. Alqarni, Group theoretical analysis for MHD flow fields: A numerical result, *J. Braz. Soc. Mech. Sci.*, **41** (2019), 1−9. https://doi.org/10.1007/s40430-019-1662-6
26. Z. Ullah, G. Zaman, A. Ishak, Magnetohydrodynamic tangent hyperbolic fluid flow past a stretching sheet, *Chinese J. Phys.*, **66** (2020), 258−268. https://doi.org/10.1016/j.cjph.2020.04.011
27. H. Sadaf, Z. Asghar, N. Iftikhar, Cilia-driven flow analysis of cross fluid model in a horizontal channel, *Comput. Part. Mech.*, **9** (2022), 1−8. https://doi.org/10.1007/s40571-022-00539-w
28. S. Arulmozhi, K. Sukkiramathi, S. S. Santra, R. Edwan, U. Fernandez-Gamiz, S. Noeiaghdam, Heat and mass transfer analysis of radiative and chemical reactive effects on MHD nanofluid over an infinite moving vertical plate, *Results Eng.*, **14** (2022), 100394. https://doi.org/10.1016/j.rineng.2022.100394
29. Y. Nawaz, M. S. Arif, K. Abodayeh, M. Mansoor, Finite difference schemes for MHD mixed convective Darcy-Forchheimer flow of Non-Newtonian fluid over oscillatory sheet: A computational study, *Front. Phys.*, **11** (2023), 16. https://doi.org/10.3389/fphy.2023.1072296
30. Y. Nawaz, M. S. Arif, K. Aboda, Predictor-corrector scheme for electrical magnetohydrodynamic (MHD) Casson nanofluid flow: A computational study, *Appl. Sci.*, **13** (2023), 1209. https://doi.org/10.3390/app13021209
31. C. S. Liu, The Lie-group shooting method for boundary-layer problems with suction/injection/reverse flow conditions for power-law fluids, *Int. J. Nonlin. Mech.*, **46** (2011), 1001−1008. https://doi.org/10.1016/j.ijnonlinmec.2011.04.016
32. W. M. K. A. D. Zaimi, B. Bidin, N. A. A. Bakar, R. A. Hamid, Applications of Runge-Kutta-Fehlberg method and shooting technique for solving classical Blasius equation, *World Appl. Sci. J.*, **17** (2012), 10−15.

33. K. U. Rehman, W. Shatanawi, U. Firdous, A comparative thermal case study on thermophysical aspects in thermally magnetized flow regime with variable thermal conductivity, *Case Stud. Therm. Eng.*, **44** (2023), 102839. https://doi.org/10.1016/j.csite.2023.102839
34. A. Usman, M. Rafiq, M. Saeed, A. Nauman, A. Almqvist, M. Liwicki, *Machine learning computational fluid dynamics*, In: 2021 Swedish Artificial Intelligence Society Workshop (SAIS), IEEE, Sweden, 2021. https://doi.org/10.1109/SAIS53221.2021.9483997
35. D. Drikakis, F. Sofos, Can artificial intelligence accelerate fluid mechanics research?, *Fluids*, **8** (2023), 212. https://doi.org/10.3390/fluids8070212
36. Z. Said, P. Sharma, R. M. Elavarasan, A. K. Tiwari, M. K. Rathod, Exploring the specific heat capacity of water-based hybrid nanofluids for solar energy applications: A comparative evaluation of modern ensemble machine learning techniques, *J. Energy Storage*, **54** (2022), 105230. https://doi.org/10.1016/j.est.2022.105230
37. A. Shafiq, A. B. Çolak, T. N. Sindhu, T. Muhammad, Optimization of Darcy-Forchheimer squeezing flow in nonlinear stratified fluid under convective conditions with artificial neural network, *Heat Transf. Res.*, **53** (2022). https://doi.org/10.1615/HeatTransRes.2021041018
38. K. U. Rehman, W. Shatanawi, Non-Newtonian mixed convection magnetized flow with heat generation and viscous dissipation effects: A prediction application of artificial intelligence, *Processes*, **11** (2023), 986. https://doi.org/10.3390/pr11040986
39. M. Adamu, A. B. Çolak, Y. E. Ibrahim, S. I. Haruna, M. F. Hamza, Prediction of mechanical properties of rubberized concrete incorporating fly ash and nano silica by artificial neural network technique, *Axioms*, **12** (2023), 81. https://doi.org/10.3390/axioms12010081
40. M. Fathizadeh, M. Madani, Y. Khan, N. Faraz, A. Yıldırım, S. Tutkun, An effective modification of the homotopy perturbation method for MHD viscous flow over a stretching sheet, *J. King Saud Univ.-Sci.*, **25** (2013), 107−113. https://doi.org/10.1016/j.jksus.2011.08.003